Supporting Information

Engineering atomic Fe-N-C with adjacent FeP nanoparticles in N, P-doped carbon for synergetic oxygen reduction and Zinc-air battery

Xiujuan Luan,[†a] Weiwei Bian,[†a] Di Guo,[†a] Bin Wang,[a*] Wei Tan,[b*] Fujun Peng,[c*] Baolong Zhou[a*]

a. School of Pharmacy, Weifang Medical University, Weifang, 261053, Shandong, PR China.

b. Department of Respiration, The First Affiliated Hospital of Weifang Medical University (Weifang People's Hospital), Weifang 261000, Shandong, PR China

c. School of Bioscience and Technology, Weifang Medical University, Weifang, 261053, PR China

E-mail: zhoubaolong@wfmc.edu.cn

[†]These authors contribute equal to this article.

Contents

Section 1. Materials and Characterization

The morphologies of powder samples were evaluated by the scan electron microscopy (SEM, ZEISS GeminiSEM 500) and the transmission electron microscopy (TEM, FEI Talos F200x) via dipping the prepared samples on a Cu-net. X-ray Photoelectron Spectroscopy (XPS) was conducted on XPSESCALAB 250Xi analyser. Powder X-ray diffraction (XRD) parameters were obtained using a Rigaku Ultima IV diffractometer at a rate of 5^{o} min^{-1} from 5^{o} to 80^{o}. Thermal gravimetric analysis (TGA) were recorded using NETZSCH STA 449C analyzer from $30^{o}C$ to $1000^{o}C$ at a heating rate of $10^{o}C$ min^{-1} under the protection of N_2. The Brunauer-Emmett-Teller (BET) method was utilized to calculate the specific surface area. The adsorption and desorption measurements for N_2 were performed on ASAP2460 (Micromeritics) at low temperature of 77 K. Pore size distributions curves were obtained from the adsorption isotherms by the non-local density functional theory (NLDFT). Total pore volumes were calculated from the uptake at a relative pressure of 0.995. Before test, all porous polymer samples were degassed overnight under high vacuum at the temperature of 150 ^{o}C to remove the solvent or the water absorbed in the porous skeleton. Raman spectra were collected from the 0 to 4000 cm^{-1} on a LabRAM HR Evolution (HORIBA) using a laser with an excitation wavelength of 532 nm. ^{1}H spectra of prepared monomers were recorded on an Avance Bruker DPX 400 (400 MHz) in the solvent of DMSO. X-ray Photoelectron Spectroscopy (XPS) was conducted on XPSESCALAB 250Xi analyser.

Section 2. Experimental Details

Synthesis of 4-hydroxyphthalonitrile (HPN).

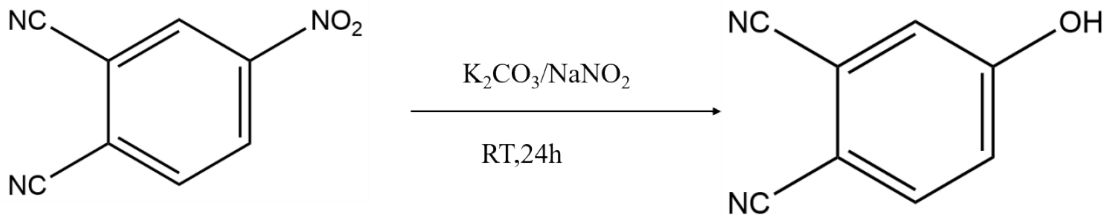

Scheme 1. Route for the synthesis of HPN

To a three-necked flask, 4-nitrophthalonitrile (3 g, 17.33 mmol), potassium carbonate (2.63 g, 19.06 mmol), Sodium nitrite (1.32 g, 19.06mmol) and 24 mL of DMSO were added. The mixture was continuously stirred at room temperature for 24 h. Then, the mixture was poured into 400 mL of dilute hydrochloric acid solution (0.1 mol/L). The precipitated gray solid was collected by suction filtration and washed with plenty of distilled water. ^{1}H-NMR (400 MHz-DMSO-d_6): 7.21 (d 1H), 7.39 (s 1H), 7.91(d 1H).

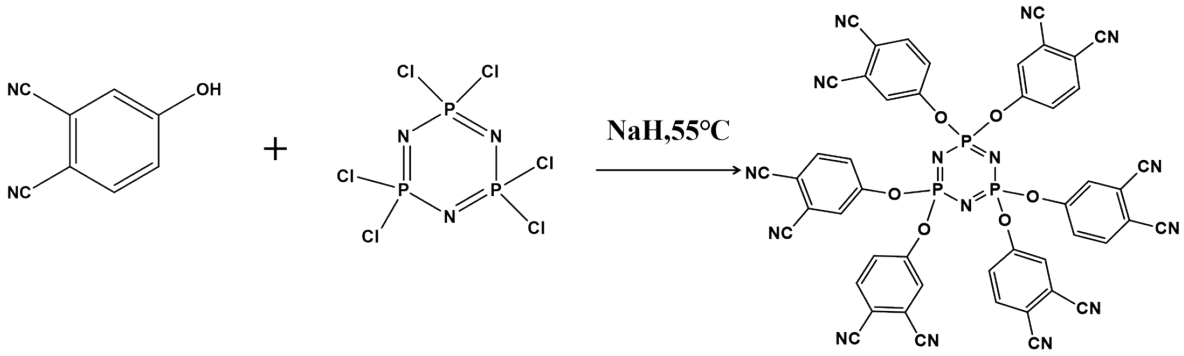

Scheme 2. Route for the synthesis of DPCP.

Phosphonitrilic chloride trimer (HCCP, 2 g, 5.75 mmol), NaH (0.83 g, 34.52 mmol), THF (86 mL), and HPN (4.97 g, 34.52 mmol) were added into a three-necked flask. The mixture was reacted at room temperature for 4 hours. Subsequently, the mixture was poured into distilled water, then which filtered and washed with water, isopropanol and propanone. The product was dried in a vacuum drying oven at 60 °C for 24 hours. ^{1}H-NMR (400 MHz-DMSO-d_6): 7.66~7.69 (d，1H), 7.98~7.99 (d 1H), 8.17~8.25(d 1H).

The preparation of FeP-CMP

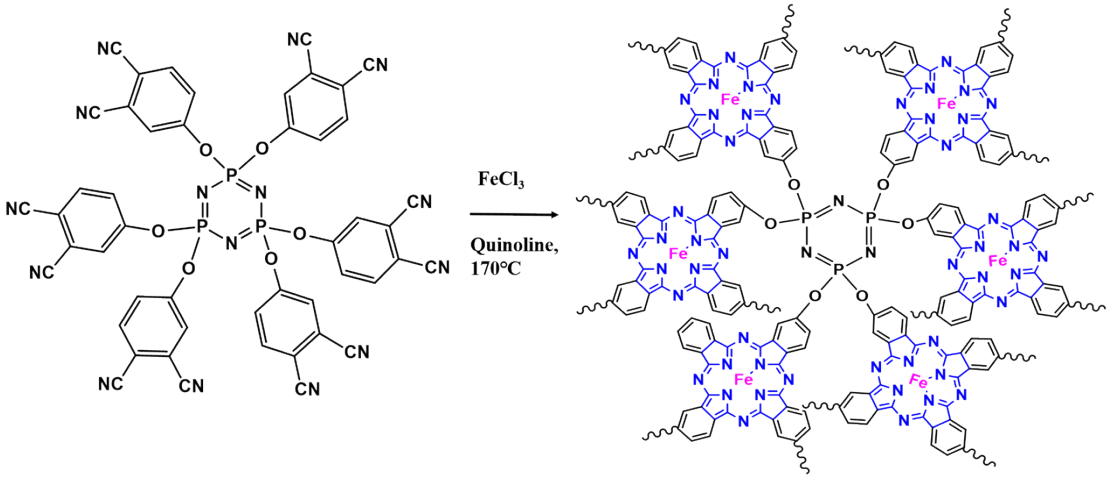

Scheme 3. Route for the synthesis of FeP-CMP.

Hexane-(3,4-dicyanophenoxy) cyclotriphosphazene（0.9934 g，1.00 mmol）and ferric chloride (0.344 g, 2.00 mmol) were stirred under Arand heated to 100 °C (15 min). Dry quinoline (7 mL) was added and the temper ature increased first to 120 °C (30 min) and then to 160°C. The reaction mixture was maintained at 160 °C for 18 h and then cooled and the precipitate filtered off. The product was washed with ethanol, dichloromethane, methanol, DMF and THF, and then extracted with THF for 24h. The product was dried in a vacuum drying oven at 100 °C to obtain the FeP-CMP powder.

The preparation of FeP-X

The as-synthesized FeP-CMP was underwent direct pyrolysis under argon at target temperatures, yielding the final catalyst denoted as FeP-X (X is the pyrolysis temperature, X=800, 900 and 1000 °C, respectively).

The preparation of FeP-900 (1:1)

Hexane-(3,4- dicyanophenoxy) cyclotriphosphazene（0.9934 g，1.00 mmol）and ferric chloride (0.172 g, 1.00 mmol) were stirred under Arand heated to 100 °C (15 min). Dry quinoline (7 mL) was added and the temper ature increased first to 120 °C (30 min) and then to 160°C. The reaction mixture was maintained at 160 °C for 18 h and then cooled and the precipitate filtered off. The product was washed with ethanol, dichloromethane, methanol, DMF and THF, and then extracted with THF for 24h. The product was dried in a vacuum drying oven at 100℃ to obtain FeP-CMP (1:1) powder.

Subsequently, the as-synthesized FeP-CMP was underwent direct pyrolysis under argon at target temperatures, yielding the final catalyst denoted as FeP-900 (1:1).

The preparation of FeP-900 (1:3)

Hexane-(3,4- dicyanophenoxy) cyclotriphosphazene（ 0.9934 g，1.00 mmol）and ferric chloride (0.4866 g, 3.00 mmol) were stirred under Arand heated to 100 °C (15 min). Dry quinoline (7 mL) was added and the temper ature increased first to 120 °C (30 min) and then to 160°C. The reaction mixture was maintained at 160 °C for 18 h and then cooled and the precipitate filtered off. The product was washed with ethanol, dichloromethane, methanol, DMF and THF, and then extracted with THF for 24h. The product was dried in a vacuum drying oven at 100℃ to obtain FeP-CMP (1:3) powder. Subsequently, the as-synthesized FeP-CMP was underwent direct pyrolysis under argon at target temperatures, yielding the final catalyst denoted as FeP-900 (1:3).

Electrochemical Measurements[1-6]

All electrochemical tests were performed using a conventional three-electrode system to measure the performance of ORR and OER at room temperature. Pt plate was used as the counter electrode, and KCl saturated Ag/AgCl or SCE (saturated calomel electrode) was used as the reference electrode. Considering the reversible hydrogen electrode (RHE) corresponded to the potentials of Ag/AgCl or SCE, the measured potentials was converted to the RHE by the Nernst equation ($E_{RHE}=E_{Ag/AgCl}+ 0.059*pH + 0.197$ V, $E_{RHE} = E_{Hg/HgO} + 0.059 *pH + 0.098$ V)[1].

The working electrode is a rotating disc electrode (RDE) consisting of a glass carbon disk (5.0 mm diameter) or a rotating ring disc electrode (RRDE) consisting of a glass carbon disk (3 mm diameter) surrounded by an outer Pt-ring (5 mm inner diameter and 7 mm outer diameter).The homogeneous catalyst ink was formed by ultrasonic oscillation of 75 μL deionized water, 375 μL ethanol, 25 μL 5wt% Nafion solution and suspension of 5 mg catalyst or 20wt% industrial Pt/C for about 0.5 h. The polished glass carbon substrate was used as the working electrode, coated with 8 μL catalyst ink, and dried naturally for about 0.5 h to prepare a uniform catalytic layer.

The catalytic activity on ORR of the catalyst was investigated by cyclic voltammetry (CV) and rotating disk electrode (RDE) at CHI-760 electrochemical station. All tests were carried out under alkaline (0.1 M KOH), neutral (0.1 M PBS) or acidic (0.1M $HClO_4$) conditions. Cyclic voltammetry (CV) was first carried out in Ar- and O_2-saturated potassium hydroxide aqueous solutions (0.1 M) at 50 mV s^{-1}. A linear sweep voltammetry (LSV) of 5 mV s^{-1} was used to measure ORR polarization curves (400 to 2500 rpm) and OER polarization curves (1600 rpm) in O_2 saturated solution. The K-L equation was applied to investigate the ORR kinetic parameters.

The electrocatalytic kinetic performance was determined with the Koutecky-Levich (K-L) formula (S1)-(S2)[2]:

$$\frac{1}{J} = \frac{1}{J_L} + \frac{1}{J_K} = \frac{1}{Bw^{1/2}} + \frac{1}{J_K} \qquad \text{(S1)}$$

In equation S1, J_L is the current that was measured; J_K represents the kinetic-limiting current and ω is the rotation speeds of electrode.[3]

$$B = 0.62nFCo(D_O)^{2/3}\ V^{1/6} \qquad \text{(S2)}$$

In equation S2, n is the total number of transferred electrons during the oxygen reduction process; F is Faradaic constant (F = 96485 C mol^{-1}), C_0 is the O_2 concentration (solubility) in 0.1 M KOH electrolyte (1.2×10^{-6} mol cm^{-3}); D_0 is the O_2 diffusion coefficient (1.90×10^{-5} cm^2 s^{-1}), and V is the kinematic viscosity of the O_2 saturated 0.1 M KOH solution (0.01 cm^2 s^{-1}).

The H_2O_2 yield and electron transfer number (N) in ORR process were measured by a rotating ring disk electrode (RRDE). The scanning rate of the disc electrode is 5 mV s^{-1}, and the calculation formula is as follows:[4-6]

$$\mathbf{H_2O_2\% = 200}\ \frac{\frac{Ir}{N}}{Id + \frac{Ir}{N}} \qquad \textbf{(S3)}$$

$$\mathbf{N = 4}\frac{Id}{Id + \frac{Ir}{N}} \qquad \textbf{(S4)}$$

In equation S3 and S4, I_d is the disk current, and Ir refers to the ring current and N represents the current collection efficiency of the Pt ring (N=0.4581).

Zn-air batteries test

To assemble the Zn-air battery, a Zn plate was used as the anode, carbon paper loaded with the catalyst was applied as the air cathode, and a mixture of 6 M KOH and 0.2 M $Zn(CH_3COO)_2$ was the electrolyte. The catalyst ink was prepared by dispersing 5 mg catalyst into 375 μL ethanol and 125 μL 5wt% Nafion aqueous solution. The mixture was then dispersed by ultrasound for 0.5 h. The ink containing 1.5 mg catalyst was loaded onto 1 cm^2 carbon paper to make the zinc-air battery. A mixture of industrial Pt/C (20%), or the mixture of Pt/C (20%) and IrO_2 with a mass ratio of 1:1 was also used as a reference air electrode. The discharge process curves were gotten via the electrochemical station (CHI760E) with a two-electrode system. Discharge-charge performance of the batteries were performed by a multichannel battery testing system (LAND CT2001A) at a current density of 10 mA cm^{-2} with 5 min discharge and 5 min charge.

Section 3. ^{1}H NMR

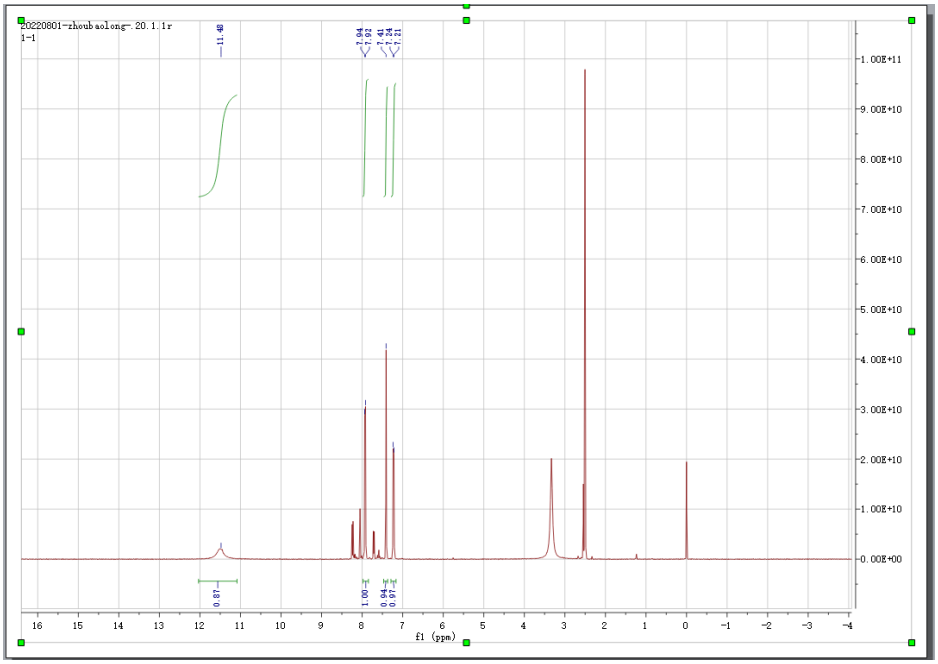

Figure S1: ^{1}H-NMR spectrum of HPN

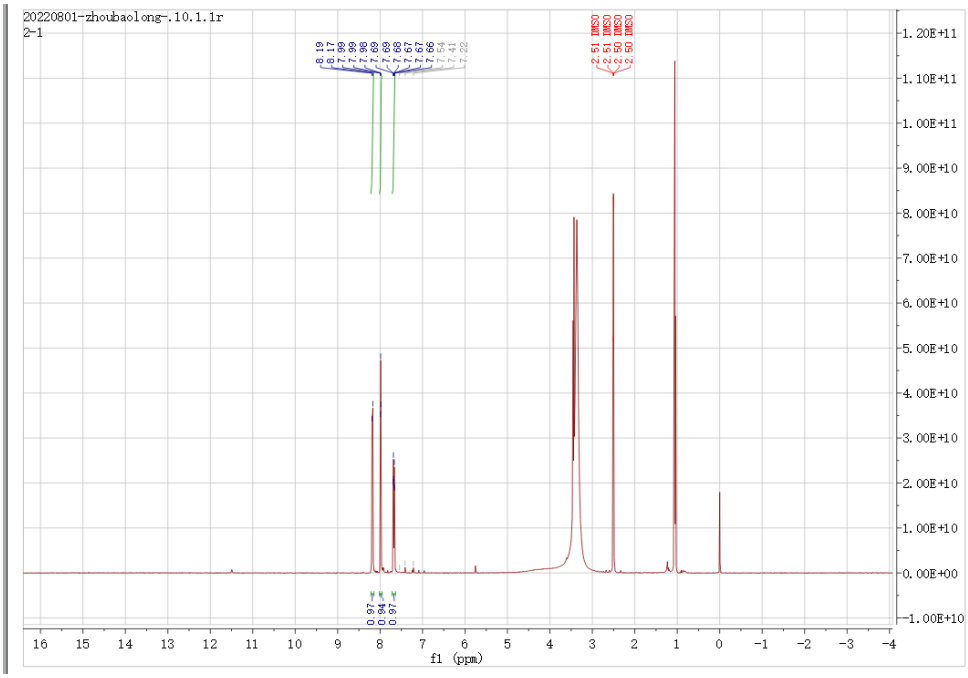

Figure S2: ^{1}H-NMR spectrum of DPCP

Section 4. FT-IR Spectra

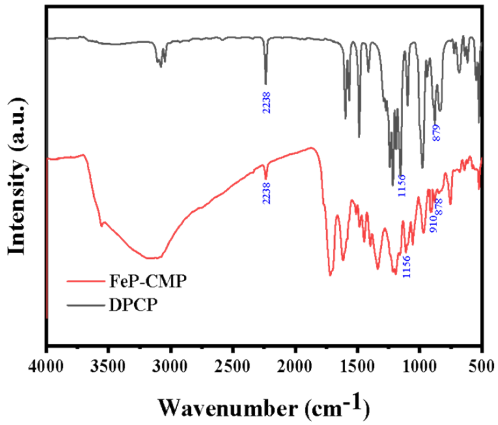

Figure S3. FTIR spectra of prepared precursors and corresponding FeP-CMP.

Section 5. TG

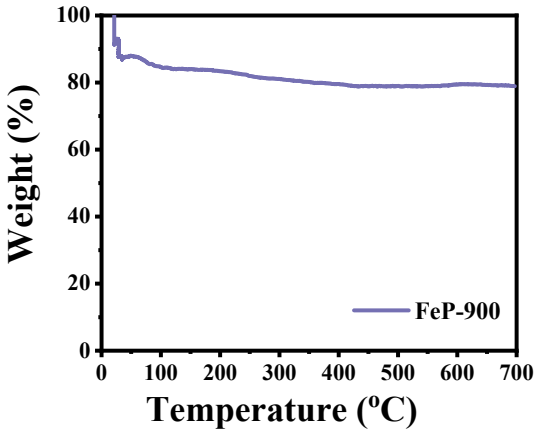

Figure S4. TGA of FeP-900 .

Section 6. XPS of FeP-X catalysts

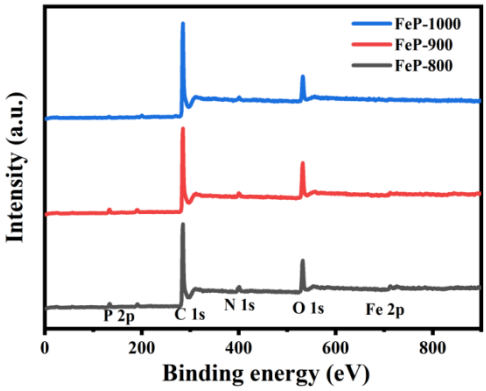

Figure S5. XPS survey of FeP-800, FeP-900 and FeP-1000 catalysts.

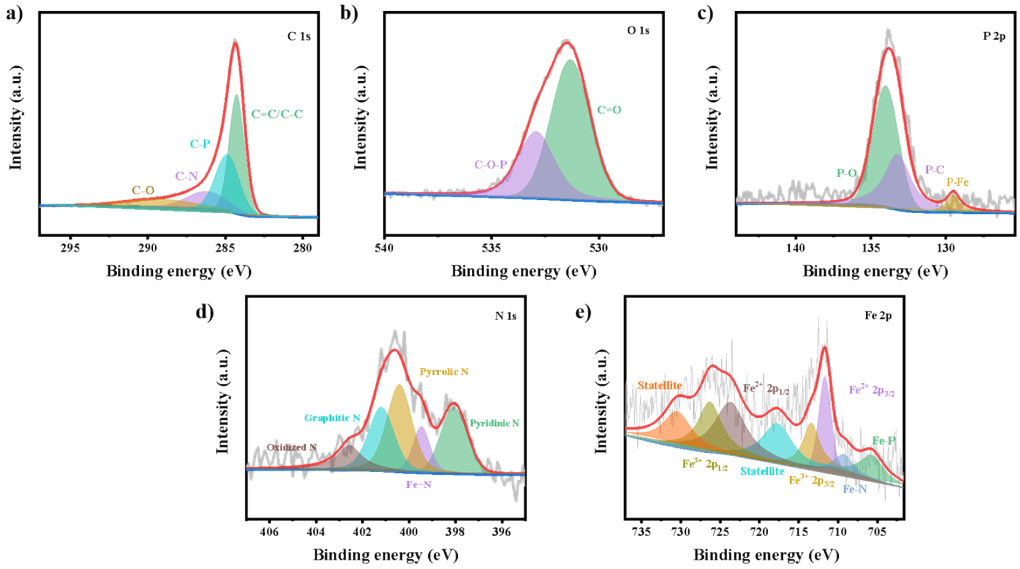

Figure S6. a) High-resolution XPS of C 1s spectra for FeP-800; b) High-resolution XPS of O 1s for FeP-800; c) High-resolution XPS spectra of P 2p spectra for FeP-800; d) High-resolution XPS spectra of N 1s spectra for FeP-800; e)High-resolution XPS spectra of Fe 2p spectra for FeP-800.

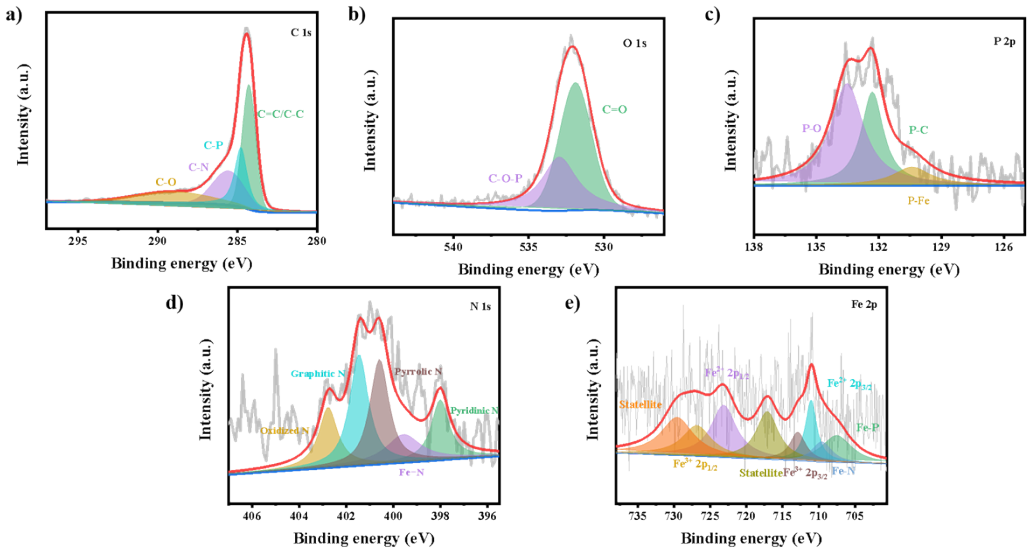

Figure S7. a) High-resolution XPS of C 1s spectra for FeP-1000; b) High-resolution XPS of O 1s for FeP-1000; c) High-resolution XPS spectra of P 2p spectra for FeP-1000; d) High-resolution XPS spectra of N 1s spectra for FeP-1000; e) High-resolution XPS spectra of Fe 2p spectra for FeP-1000.

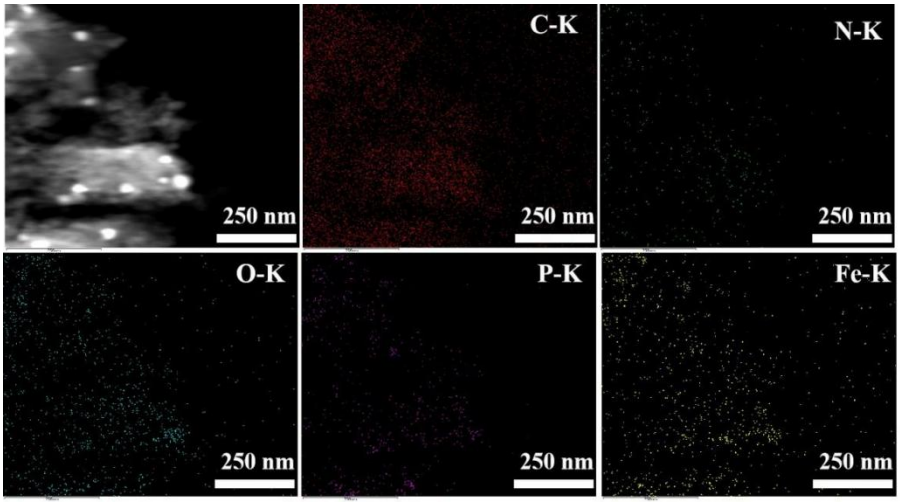

Figure S8. Element mappings of FeP-900 at a scale bar of 250 nm.

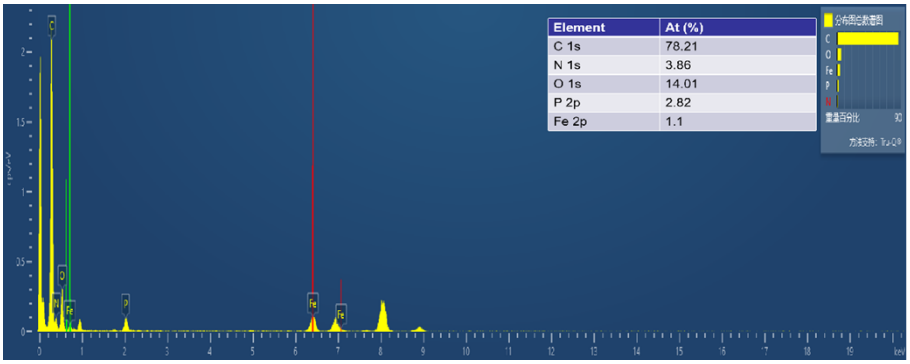

Figure S9. EDS spectra of FeP-900.

Section 7. Electrochemical Performance

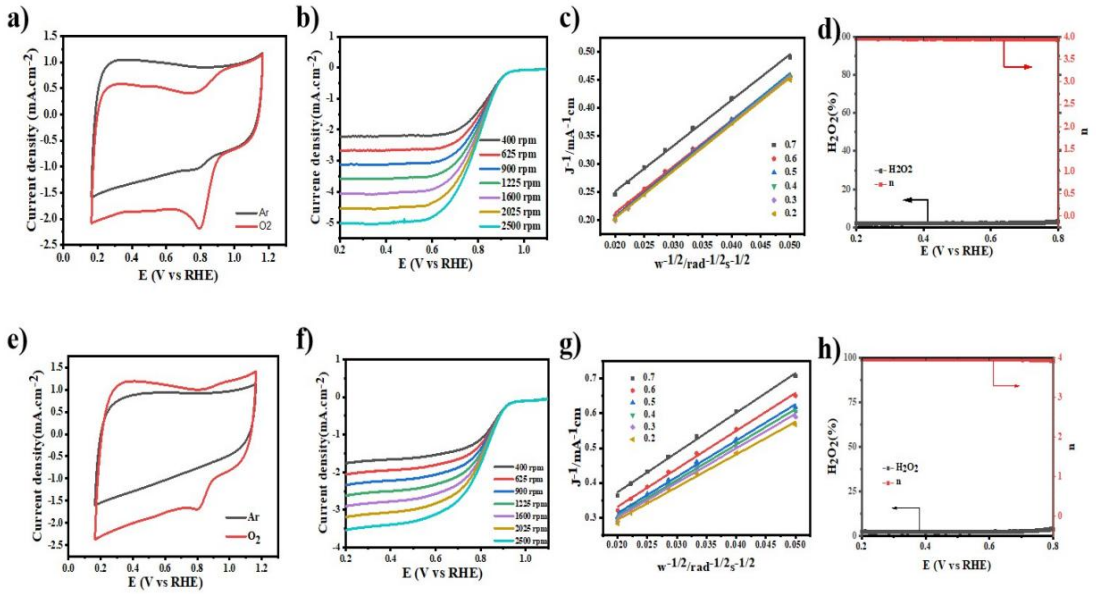

Figure S10. a) CV curves of FeP-900 (1:1) on a glassy carbon electrodes in 0.1 M KOH saturated with O_2 or Ar at a sweep rate of 50 mV s-1; b) LSV of FeP-900 (1:1) at various rotation speeds; c) K-L plots curves of FeP-900 (1:1); d) Percentage of hydrogen peroxide yield and the electron transfer number (n) of FeP-900 (1:1) ; e) CV curves of FeP-900 (1:3) on a glassy carbon electrodes in 0.1 M KOH saturated with O_2 or Ar at a sweep rate of 50 mV s-1; b) LSV of FeP-900 (1:3) at various rotation speeds; c) K-L plots curves of FeP-900 (1:3); d) Percentage of hydrogen peroxide yield and the electron transfer number (n) of FeP-900 (1:3).

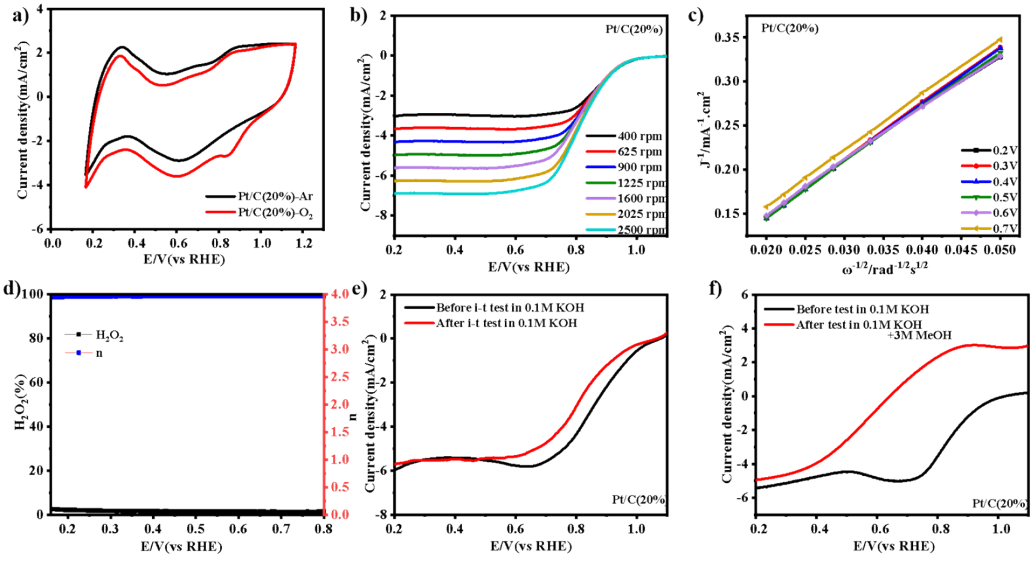

Figure S11. a) CV curves of commercial Pt/C (20%) on a glassy carbon electrodes in 0.1 M KOH saturated with O_2 or Ar at a sweep rate of 50 mV s-1; b) LSV of commercial Pt/C (20%) at various rotation speeds; c) K-L plots curves of commercial Pt/C (20%); d) Percentage of hydrogen peroxide yield and the electron transfer number (n) of Pt/C at different potentials; e) Polarization curves of Pt/C (20%) measured by RDE in O_2-saturated 0.1 M KOH before (black line) and after (red line) the i-t (20000 s) experiments; f) LSV curve of Pt/C measured before and after the injection of 3 M methanol.

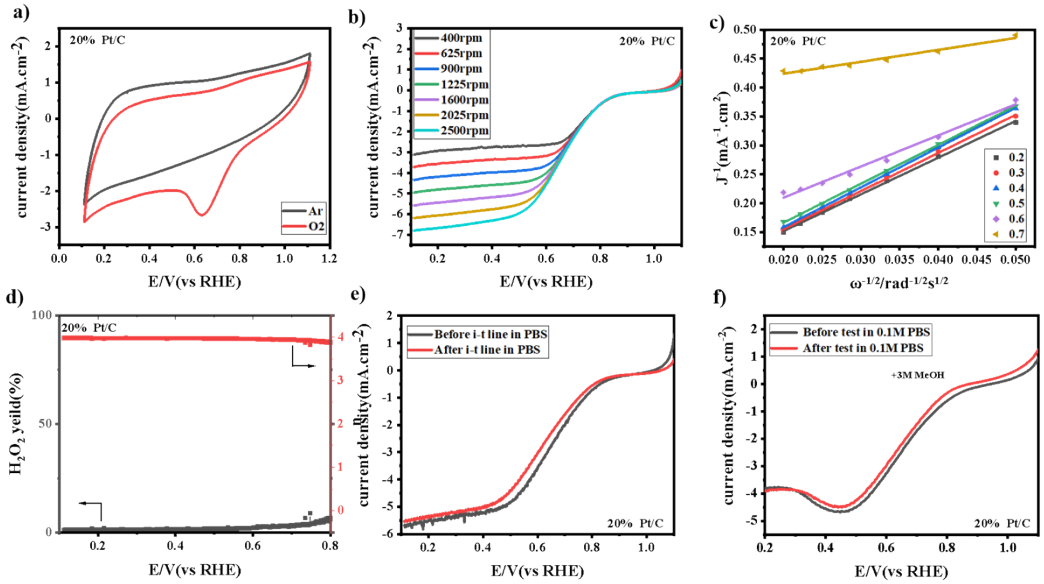

Figure S12. Electrochemical performance of commercial Pt/C in neutral conditions. a) CV curves of commercial Pt/C (20%) on glassy carbon electrodes in water solution of 0.1 M PBS saturated with O_2 or argon at a sweep rate of 50 mV s-1. b) LSV of commercial Pt/C (20%) at different rotation speeds; c) K-L plots curves of Pt/C (20%) at different potentials; d) Percentage of hydrogen peroxide yield and the electron transfer number (n) of Pt/C (20%) at different potentials; e) Polarization curves of Pt/C (20%) measured by RDE in O_2-saturated 0.1 M PBS before (black line) and after (red line) the i-t (20000 s) experiments; f) LSV curve of Pt/C (20%) measured before and after the injection of 3 M methanol.

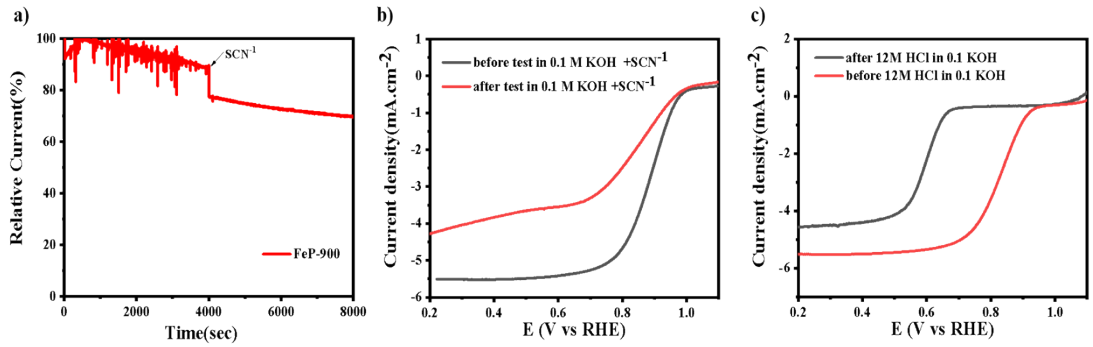

Figure S13. a) Current-time (i-t) curves; b) RDE results of FeP-900 in O_2-saturated 0.1 M KOH solution (without and with SCN^{-1}); c) RDE result of FeP-900 in O_2-saturated 0.1 M KOH solution (before and after treatment with 12M HCl hydrochloric acid.

Figure S14. Open-circuit voltage (OCV) plots

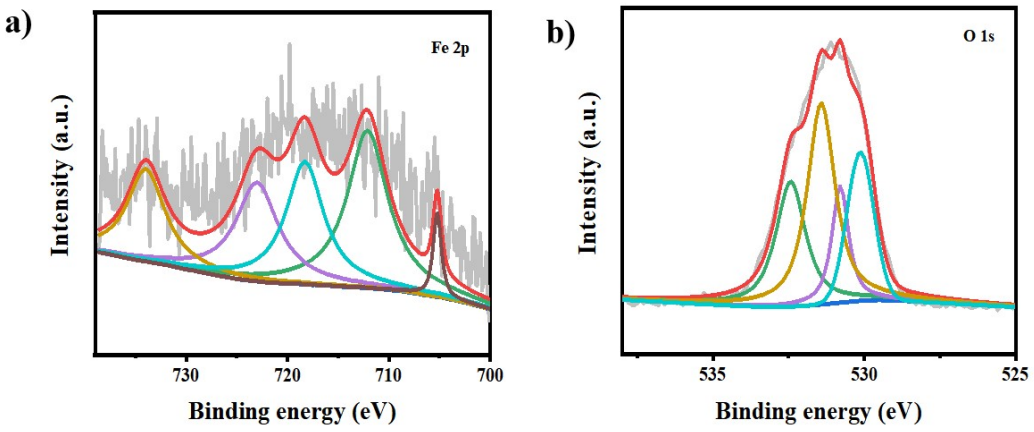

Figure S15. Fe 2p spectrum analysis of a zinc-air battery FeP-900 after long time charge and discharge operation

Section 8. Supporting Tables

Table S1. Porosity Parameters of prepared corresponding catalysts

Sample	BET (m^2/g)	V_{total} (cm^3/g)	V_{micro} (cm^3/g)	Mean Pore diameter(nm)
FeP-800	518.4	0.2398	119.11	1.8502
FeP-900	959.16	0.7216	220.37	3.0095
FeP-1000	551.94	0.4465	126.81	3.2361

Table S2. The surface element contents of different species including carbon, oxygen, nitrogen, cobalt and iron in as-synthesized catalysts, calculated from the XPS spectra

Sample	C (Atomic%)	N (Atomic%)	O (Atomic%)	P (Atomic%)	Fe (Atomic%)
FeP-800	77.67	5.03	13.42	2.74	1.13
FeP-900	78.21	3.86	14.01	2.82	1.1
FeP-1000	84.87	3.02	10.48	1.04	0.6

Table S3. The surface contents of different N species in FeP-900 catalysts, calculated from the XPS spectra

Sample	Pyridinc N in total N (%)	Fe-N in total N (%)	Pyrrolic N in total N (%)	Graphitic N in total N (%)	Oxidized N in total N (%)
FeP-800	22.01	11.28	31.69	23.49	11.53
FeP-900	17.31	17.39	17.60	29.58	18.43
FeP-1000	18.04	16.41	31.65	34.29	19.18

Table S4. Summary of various electrocatalysts for ORR in 0.1 M KOH.

Catalyst	E_{Onset} (V)	$E_{1/2}$ (V)	n	Reference
FeP-900	**0.98**	**0.82**	**3.97**	**This work**
Fe-NC	0.96	0.88	3.80	ref. [7]
Fe/N/S-CNTs	0.99	0.89	/	ref. [8]
Co/CoNx/N-CNT/C	0.90	0.80	3.77	ref. [9]
CoFeNx/C	1.01	0.87	3.5	ref. [10]
Fe_{SA}/NSC	1.01	0.91	3.99	ref. [11]
(Fe, Co)@NGC	0.91	0.85	3.70	ref. [12]
Fe@C-NG/NCNTs	0.93	0.84	/	ref. [13]
Fe/SNC	0.85	0.77	3.85	ref. [14]

Table S5. Summary of various electrocatalysts for ORR in 0.1 M PBS

Catalyst	Onset potential (V vs. RHE)	ORR Half-wave potential (V vs. RHE)	n	Ref.
FeP-900	**0.846**	**0.70**	**3.96**	**This work**
Fe-P-C	0.84	0.52	3.80	ref. [15]

HFCP-850	0.83	0.60	3.94	ref. [16]
CP-CMP-900	0.906	0.73	3.95	ref. [17]
Fe-P-C	0.84	0.52	3.8	ref.[18]
Fe-N/C-800	0.72	0.55	3.97	ref. [19]
BP-800	0.85	0.66	3.79	ref. [20]
FeIM/ZIF-8	0.91	0.75	3.70	ref. [21]

Table S6. Comparison of zinc-air battery utilizing H-PZS-Fe-850 with other noble-metal free electrocatalysts reported recently.

Catalysts	**Peak power ($mW\ cm^{-2}$)**	**energy density ($mA\ h\ g^{-1}_{Zn}$)**	**Ref.**
FeP-900	208	801	This work
FexN/NC-7	180	668	Ref.[22]
FeS_2-CoS_2	257	814	Ref.[23]
2D Fe-N-C	320	798	Ref.[24]
$FeNi_{3@}$NC	139	756	Ref.[25]
FeNC-Fe_xC/Fe	149	663	Ref.[26]
Co@NC	105	768	Ref.[27]
Fe-N-HPC	165	735	Ref.[28]

Section 9. Supporting References

1. Z. Zhang, J. Sun, M. Dou, J. Ji, F. Wang, *ACS Appl. Mater. Interfaces*. 2017, 9, 16236-16242.
2. Z. Xiang, Y. Xue, D. Cao, L. Huang, J.F.Chen, L. Dai, *Angew. Chem. Int. Ed.*, 2014, 53, 2433-2437.
3. S.Ren,J.Wang, X. Xia, *Mater. Interfaces.* 2016, 8, 25875-25880.
4. J. Hao, S. Zhang, R. Liu, J. Ning,G. Zhang, L. Zhi, *Adv. Mater.*, 2015, 27, 3190-3195.
5. K. Hu, Z. Xiao, Y.Cheng, D.Yan, R.Chen, J. Huo, S. Wang, *Electrochim. Acta.* 2017, 254,

280-286.

6. K. P. Singh,E. J. Bae, J.Yu, J. Am. *Chem. Soc.*, 2015, 137, 3165-3168.
7. Y. Wang, Y. Pan, L. Zhu, H. Yu, B. Duan, R. Wang, Z. Zhang, S. Qiu, *Carbon N. Y.*, 2019, 146, 671-679.
8. H. Jin, H. Zhou, W. Li, Z. Wang, J. Yang, Y Xiong, D. He, L. Chen, S. Mu. *J. Mater. Chem. A.*, 2018, 6, 20093-20099
9. H. Zhong, Y. Luo, S. He, P. Tang, D. Li, N. Alonso-Vante and Y. Feng, *ACS Appl. Mater. Interfaces*, 2017, 9, 2541–2549.
10. R. Jiang and D. Chu, *J. Power Sources*, 2014, **245**, 352–361.
11. X. Liu, X. Zhai, W. Sheng, J. Tu, Z. Zhao, Y. Shi, C. Xu, G. Ge, X. Jia, *J. Mater. Chem. A*, 2021, 9, 10110-10119.
12. J. Xi, Y. Xia, Y. Xu, J. Xiao and S. Wang, *Chem. Commun.*, 2015, 51, 10479–10482.
13. Q. Wang, Y. Lei, Z. Chen, N. Wu, Y. Wang, B. Wang, Y. Wang, *J. Mater. Chem. A*, 2018, 6, 516- 526.
14. H. Shen, E. Gracia-Espino, J. Ma, K. Zang, J. Luo, L. Wang, S. Gao, X. Mamat, G. Hu, T. Wagberg, S. Guo, *Angew. Chem. Int. Ed.*, 2017, 56, 13800-13804.
15. K. P. Singh, E. J. Bae and J.S. Yu, *J. Am. Chem. Soc.*, 2015, **137**, 3165–3168.
16. J. Dou, M. Qi, H. Wang, W. Shi, X. Luan, W. Guo, L. Xiao, C. Zhao, D. Cheng, T. Jiang, W. Zhang, W. Bian, B. Zhou, *Micropor. Mesopor. Mater.*, 2021, 320, 111101.
17. M. Zhang, J. Ming, W. Zhang, J. Xie, P. Lin, X. Song, X. Chen, X. Wang, B. Zhou, *ACS Omega*, 2020,5, 7225-7234.
18. K. P. Singh, E. J. Bae and J.S. Yu, *J. Am. Chem. Soc*., 2015, 137, 3165–3168.
19. L. Lin, Q. Zhu and A.-W. Xu, *J. Am. Chem. Soc.*, 2014, **136**, 11027–11033.
20. K. P. Singh, E. J. Bae and J.S. Yu, J. Am. Chem. Soc., 2015, 137, 3165–3168.
21. J. Dou, H. Luo, C. Zhang, J. Lu, X. Luan, W. Guo, T. Zhang, W. Bian, J. Bai, X. Zhang and B. Zhou, *New Journal of Chemistry*, 2021, **45**, 21020-21030.
22. D. Zhao, J.L. Shui, C. Chen, X. Chen, B. M. Reprogle, D. Wang and D.-J. Liu, *Chem. Sci.,* 2012, **3**, 3200–3205.
23. X. Hu, Y. Min, L.-L. Ma, J.-Y. Lu, H.-C. Li, W.-J. Liu, J.-J. Chen, H.-Q. Yu, *Appl. Catal. B*,

2020, 268,118405.

24. X. Shi, B. He, L. Zhao, Y. Gong, R. Wang, H. Wang, *J. Power Sources*, 2021, 482, 228955.
25. R. Yuan, W. Bi, T. Zhou, N. Zhang, C.a. Zhong, W. Chu, W. Yan, Q. Xu, C. Wu, Y. Xie, *Mater. Lett.*, 2019, 2, 35-41.
26. D. Chen, J. Zhu, X. Mu, R. Cheng, W. Li, S. Liu, Z. Pu, C. Lin, S. Mu, *Appl. Catal. B,* 2020, 268, 118729.
27. Y. Qiao, P. Yuan, Y. Hu, J. Zhang, S. Mu, J. Zhou, H. Li, H. Xia, J. He, Q. Xu, *Adv. Mater.,* 2018, 30, 1804504.
28. S.S. Shinde, C.H. Lee, J.-Y. Jung, N.K. Wagh, S.-H. Kim, D.-H. Kim, C. Lin, S.U. Lee, J.-H. Lee, *Energy Environ. Sci.* 2019, 12, 727-738.
29. D. Wang, H. Xu, P. Yang, L. Xiao, L. Du, X. Lu, R. Li, J. Zhang, M. An, *J. Mater. Chem.A,* 2021, **9**, 9761-9770.